



Ayres, J. D. S., Čulo, M., Buhot, J., Carrington, A., Friedemann, S., Hussey, N. E., & et, A. (2022). Transport evidence for decoupled nematic and magnetic criticality in iron chalcogenides. *Communications Physics*, 5(1), [100]. <https://doi.org/10.1038/s42005-022-00873-8>

Publisher's PDF, also known as Version of record

License (if available):
CC BY

Link to published version (if available):
[10.1038/s42005-022-00873-8](https://doi.org/10.1038/s42005-022-00873-8)

[Link to publication record in Explore Bristol Research](#)
PDF-document









This is the final published version of the article (version of record). It first appeared online via Nature Research at <https://doi.org/10.1038/s42005-022-00873-8>. Please refer to any applicable terms of use of the publisher.

University of Bristol - Explore Bristol Research

General rights

This document is made available in accordance with publisher policies. Please cite only the published version using the reference above. Full terms of use are available: <http://www.bristol.ac.uk/red/research-policy/pure/user-guides/ebr-terms/>

Transport evidence for decoupled nematic and magnetic criticality in iron chalcogenides

Jake Ayres^{1,2}[✉], Matija Čulo^{2,5}, Jonathan Buhot^{1,2}, Bence Bernáth², Shigeru Kasahara³, Yuji Matsuda³, Takasada Shibauchi⁴, Antony Carrington¹, Sven Friedemann¹ & Nigel E. Hussey^{1,2}[✉]

Electronic nematicity in correlated metals often occurs alongside another instability such as magnetism. The question thus remains whether nematicity alone can drive unconventional superconductivity or anomalous (quantum critical) transport in such systems. In FeSe, nematicity emerges in isolation, providing a unique opportunity to address this question. Studies to date, however, have proved inconclusive; while signatures of nematic criticality are observed upon sulfur substitution, they appear to be quenched by the emergent magnetism under the application of pressure. Here, we study the temperature and pressure dependence of the low-temperature resistivity of FeSe_{1-x}S_x crystals at x values beyond the nematic quantum critical point. Two distinct components to the resistivity are revealed; one that is suppressed with increasing pressure and one that grows upon approaching the magnetic state at higher pressures. These findings hint that nematic and magnetic critical fluctuations in FeSe_{1-x}S_x are completely decoupled, in marked contrast to other Fe-based superconductors.

¹H. H. Wills Physics Laboratory, University of Bristol, Tyndall Avenue, Bristol BS8 1TL, United Kingdom. ²High Field Magnet Laboratory (HFML-EMFL) and Institute for Molecules and Materials, Radboud University, Toernooiveld 7, 6525 ED Nijmegen, Netherlands. ³Department of Physics, Kyoto University, Sakyo-ku, Kyoto 606-8502, Japan. ⁴Department of Advanced Materials Science, University of Tokyo, Kashiwa, Chiba 277-8561, Japan. ⁵Present address: Institut za fiziku, P.O. Box 304, HR-10001 Zagreb, Croatia. ✉email: jake.ayres@bristol.ac.uk; n.e.hussey@bristol.ac.uk

A common characteristic of unconventional superconductors is their proximity to another ground state of broken symmetry, fluctuations of which can both mediate superconductivity and drive non-Fermi-liquid (nFL) behavior in the vicinity of its associated quantum critical (QC) point. Nematicity—a lowering of rotational symmetry without breaking translational symmetry—is one form of order that has been observed in a variety of systems, including iron-based^{1–3}, cuprate⁴, heavy fermion⁵, and Moiré⁶ superconductors. The extent to which nematic order and its fluctuations are responsible for pairing and QC phenomena has proved a challenging question, however, largely due to the fact that nematicity often occurs in the vicinity of another, possible primary, instability. In iron-pnictides, for example, nematicity is claimed to be a spin-driven effect⁷ while QC phenomena observed in Sr₃Ru₂O₇—initially attributed to a nematic quantum critical point (NQCP)⁸—were later found to arise in the presence of a field-tuned spin-density wave⁹.

FeSe is unusual in that nematic order stabilizes in the absence of static magnetism³. Below a tetragonal-to-orthorhombic distortion at $T_s = 90$ K, both its normal¹⁰ and superconducting (SC)¹¹ state properties exhibit marked two-fold anisotropy. Although widely believed to be electronic in origin¹², it remains unclear whether the nematic transition is driven by charge¹³, orbital¹⁴, or magnetic¹⁵ correlations. Nevertheless, its discovery offers a unique opportunity to test theoretical predictions for nFL or “strange metallic” behavior arising solely from critical nematic fluctuations^{16–22}. To this end, a large effort has been made to elucidate the respective roles of nematic and magnetic fluctuations in shaping the normal and SC properties of FeSe^{23–26}.

High-pressure studies on FeSe have proved to be highly instructive in this pursuit. As pressure increases, T_s is suppressed (to $T_s = 0$ K at $p = p_c$) but the SC transition temperature T_c is not enhanced at p_c ²⁷. Beyond the nematic state ($p > p_c$), however, there is a marked (four-fold) increase in T_c ^{27–29} that has been naturally linked to strengthening magnetic interactions³⁰. The role of nematicity in driving nFL/QC phenomena has proved more controversial. At $p = p_c$, the critical nematic fluctuations in FeSe are quenched¹³, presumably due to the emergence of long-range magnetic order before the nematic phase terminates³¹. In FeSe_{1–x}S_x, nematicity is also suppressed with increasing sulfur substitution, vanishing at a critical S concentration $x_c = 0.17$ ³² where the nematic susceptibility also diverges¹² and quantum critical transport is observed³³. Since no magnetic order develops at any point across the substitution series (at ambient pressure), this divergence suggests that a genuine NQCP exists in FeSe_{1–x}S_x.

The question remains, however, whether the emergent critical nematic fluctuations are responsible for the strange metal transport seen at ambient pressure in FeSe_{1–x}S_x^{33–38}. Although static magnetism is not stabilized at ambient pressure, low-energy spin-fluctuations, for example, are known to persist to $p = 0$ at low T and low x ³⁹. Moreover, quantum oscillation studies indicating a lack of divergence in the effective mass m^* on approaching the NQCP⁴⁰ have led to the suggestion that the critical nematic fluctuations may also be quenched at ambient pressure—in this case, due to nemato-elastic coupling or local strain effects^{41,42}—the nFL transport then being attributed to scattering of the residual spin fluctuations. To date, however, the full evolution of $m^*(x)$ from $x = 0$ to $x > x_c$ is only known for a single oscillation frequency⁴⁰ leaving open the question of whether or not mass enhancement occurs at other locations on the Fermi surface.

With increasing x , p_c falls while p_m , the onset pressure for magnetic order, increases⁴³, leading ultimately to a separation of the nematic and magnetic phases in the (p , T) plane at higher x . Previous NMR measurements appeared to confirm such a separation at $x = 0.12$ ($< x_c$)⁴⁴. Detailed transport studies⁴⁵ on

pressurized FeSe_{1–x}S_x with $x = 0.11$ then revealed the absence of nFL transport or m^* enhancement across p_c , supporting the picture of quenched nematic criticality due to strong nemato-elastic coupling⁴⁵. A more recent μ SR study, however, found that magnetism at $x = 0.11$ is stabilized before nematicity is destroyed (the discrepancy between μ SR and NMR likely reflects the different timescales of the two probes)⁴⁶. Hence, it is unclear whether the suppression of nematic criticality near $x = 0.12$ under pressure is due to coupling to the lattice or to slowly fluctuating moments. In order to determine whether critical nematic fluctuations alone can drive nFL transport in FeSe_{1–x}S_x, pressure studies on samples with higher x values, where the nematic and magnetic phases are fully separated, are required.

Here, we study the low- T resistivity $\rho(T)$ of FeSe_{1–x}S_x with $x = 0.18$ and 0.20 ($> x_c$) under applied pressures up to 15 kbar ($< p_m$). Whilst the form of $\rho(T)$ cannot differentiate easily between nematic and magnetic fluctuations, tracking its evolution with p may reveal an approach to or a retreat from a QCP associated with either order parameter. In this way, their respective influences can be disentangled. For both samples studied here, we find two distinct T^2 components in $\rho(T)$ (due to quasiparticle-quasiparticle scattering) which extend over different T ranges and whose coefficients show contrasting p -dependencies. The term that grows with increasing p is attributed to the dressing of quasiparticles by critical magnetic fluctuations that strengthen upon approach to the magnetic QCP^{43,47}. Its coefficient at ambient pressure, however, is found to be negligible. This implies that the source of the large and strongly x -dependent T^2 coefficient observed at ambient pressure is the scattering of quasiparticles that are dressed purely by the orbital nematic fluctuations. Finally, this coexistence of two distinct components to $\rho(T)$ also suggests that, in contrast to what is observed in the iron-pnictides, the critical nematic and magnetic fluctuations in FeSe_{1–x}S_x are completely decoupled.

Results

Nematic quantum critical resistivity. Figures 1a, b show, respectively, the zero-field $\rho(0, T)$ (pale) and high-field $\rho(35 \text{ T}, T)$ curves for samples with nominal x values of 0.18 and 0.20 oriented $\mathbf{H} // \mathbf{I} // ab$ at various pressures $0 \leq p \leq 14.4$ kbar. The suppression of superconductivity by the magnetic field is apparent in all data sets. For $T > T_c$, there is almost complete overlap between $\rho(0, T)$ and $\rho(35 \text{ T}, T)$, confirming that the magnetoresistance in this field orientation is negligible beyond x_c ^{33,36}, in marked contrast to the large magnetoresistance seen for $\mathbf{H} // c$ ^{35,36}. The broadening and structure of the superconducting transitions in $\rho(0, T)$ is highly reproducible between subsequent cooldowns at different pressures, between samples of similar dopings⁴⁸, and between measurements performed by different groups^{47,49} indicating that non-hydrostaticity is unlikely to be playing a role here. We also note that the transitions sharpen again at higher pressures (~ 3 GPa)⁴³ suggesting that this behavior is in fact intrinsic.

The corresponding derivatives $d\rho/dT(35 \text{ T})$ of the high-field curves, shown in panels c and d of Fig. 1, reveal a systematic evolution of $\rho(T)$ under applied pressure. To better orientate our discussion, we focus initially on the form of $d\rho/dT$ at ambient pressure. For $T < 10$ K, $\rho(35 \text{ T}, T) = \rho_0 + A_1 T^2$ with A_1 coefficients that are determined by fitting the $d\rho/dT$ traces at the lowest temperatures to a straight line through the origin (black lines in Figs. 1c, d). The temperature range fitted to was chosen in order to avoid being influenced by the clear crossover in behavior that occurs at ~ 10 K and the pressure-induced enhancement of superconductivity at the lowest temperatures. We argue below that A_1 reflects the total quasiparticle-quasiparticle scattering cross-section enhanced by both magnetic and nematic critical

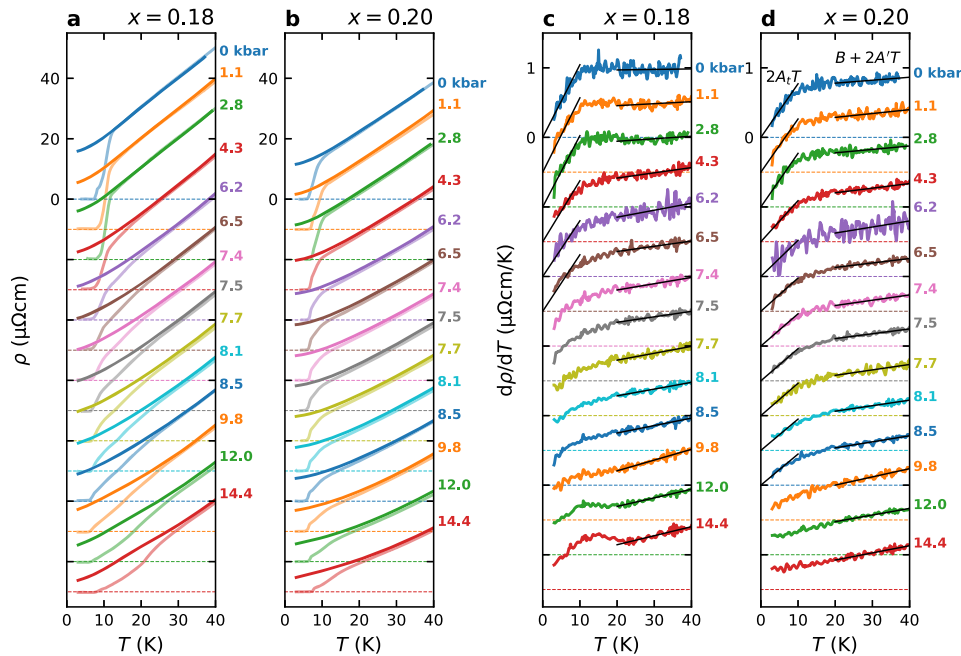


Fig. 1 Pressure dependence of the high-field in-plane resistivities of $\text{FeSe}_{1-x}\text{S}_x$ beyond the nematic quantum critical point. **a, b** Zero-field resistivity $\rho(0, T)$ (pale curves) and high-field resistivity $\rho(35 \text{ T}, T)$ (dark curves) measured at indicated pressures p between 0 and 14.4 kbar for $x = 0.18$ ($x = 0.20$) and up to a temperature T of 40 K with magnetic field H and current I both oriented in-plane and parallel to each other ($\mathbf{H}/I//ab$). The curves have been offset by $10 \mu\Omega \text{ cm}$ for each subsequent pressure for clarity. **c, d** Corresponding first derivatives of the high-field resistivity for doping $x = 0.18$ ($x = 0.20$) at the same pressures as those in **a, b**. For clarity, the curves have been offset by $0.5 \mu\Omega \text{ cm K}^{-1}$ at each pressure. The dashed lines indicate the $\rho = 0$ or $d\rho/dT = 0$ position of each curve. In panels **c, d**, the black lines are straight-line fits to the lowest temperature data chosen to both avoid the crossover to $T + T^2$ behavior at ~ 10 K and the onset of superconductivity at low temperatures and to the higher temperature data above 20 K from which the resistivity coefficients A_t (A), B , and A' have been deduced. The enhancement of superconductivity prevents A_t from being determined at the highest applied pressures. The increasingly broad superconducting transitions manifest themselves as shallow peaks in the derivatives that are most visible in $d\rho/dT$ ($x = 0.18$) above 9.8 kbar (panel **c**) but may influence the data at lower pressures as well. The fits at low- T have been forced through the origin. The small finite intercepts due to superconductivity at intermediate pressures are accounted for in the errors.

fluctuations. Above the T^2 regime, $d\rho/dT$ is essentially flat, implying that $\rho(T)$ becomes T -linear (with coefficient B). Such a T^2 to T -linear crossover is characteristic of a metallic system in the vicinity of a QCP^{1,50–53}.

Pressure-induced growth of a purely T^2 component. A notable change in the derivative plots with increasing p is the emergence of a finite linear slope in $d\rho/dT$ at higher temperatures, indicative of a second T^2 component that (i) coexists with the T -linear term, (ii) has a coefficient A' that is around one order of magnitude smaller than A_t , and (iii) extends over a much broader temperature range. A' and B are determined by fitting the $d\rho/dT$ data between 20 and 40 K to another straight line (high- T black lines in Fig. 1c, d). The fitting range was increased to 25 to 40 K for $x = 0.18$ at the highest pressures to again avoid being influenced by the onset of superconductivity. Whilst this second T^2 component is most evident in the derivative data at high T , the expectation is, as for a correlated Fermi liquid, that it extends down to the lowest temperatures. In this way, A_t is most naturally interpreted as the sum of two T^2 components, i.e., $A_t = A + A'$; the first component persisting up to ~ 10 K, the second component up to the highest temperature measured in our study (~ 40 K).

The p -dependence of coefficients A (A_t), B , and ρ_0 (the latter obtained by extrapolating fits of the low- T $\rho(T)$ curves at 35 to 0 K) is shown in Fig. 2a–c, respectively. It is immediately apparent that the relative slopes of all three quantities are the same, indicating that their p -dependencies share a common origin. The p -dependence of A' and T_c is shown in Fig. 2d, e respectively. The

strong anticorrelation of $A'(p)$ with $A(p)$ and $B(p)$ indicates that its origin is distinct. It, therefore, appears that there are two distinct components: one that crosses from T^2 (with coefficient A) to T -linear (with coefficient B) and a second that remains purely T^2 up to at least 40 K (with coefficient A').

Carrier density inferred from the residual resistivity. The drop in A (A_t), B , and ρ_0 with increasing pressure could signify either a reduction in scattering or an increase in the plasma frequency ω_p^2 (i.e., n/m^*), or some combination thereof. In the first scenario, the fall in A (A_t), B , and ρ_0 with increasing p (depicted in Fig. 2) would be attributed directly to a reduction in the dressing of quasiparticles by the relevant critical fluctuations. While this interpretation can support a typical quantum critical scenario in which $A(p)$ (and perhaps ρ_0) drops as the system is tuned away from the NQCP, the scattering rate associated with the linear-in- T coefficient is not expected to decrease too. Indeed, the T -linear resistivity inside of the quantum critical fan in $\text{FeSe}_{1-x}\text{S}_x$ at ambient pressure has been shown to be governed by a doping-independent scattering rate $1/\tau$ that is tied to the Planckian limit, i.e., $\hbar/\tau = ak_B T$ with $1 \leq a \leq 2$ ³³.

In the second scenario, the change in all three coefficients can be ascribed wholly to an increase in n/m^* . A sizeable increase in n with pressure has been deduced in both FeSe ⁵³ and $\text{FeSe}_{0.89}\text{S}_{0.11}$ ⁴⁵ from quantum oscillation studies. Indeed, for $x = 0.11$, six of the eight observed oscillation frequencies (corresponding to the largest Fermi pockets) increase appreciably (50–75%) between 0 and 17 kbar⁴⁵. To account for this, a rescaling factor $\rho_0(0)/\rho_0(p)$ (dashed lines in Fig. 2c) can be found that assumes the decrease in

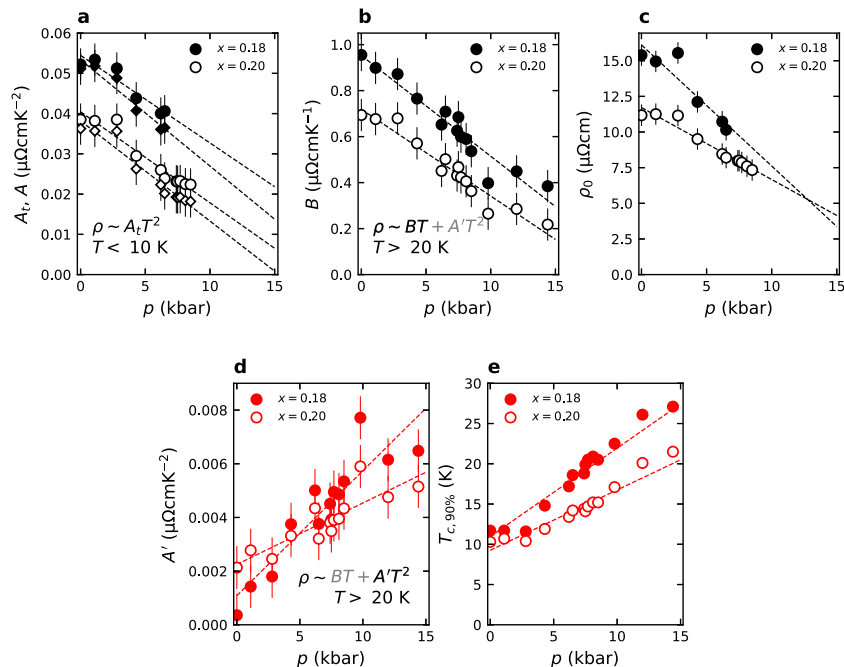


Fig. 2 Pressure dependence of the resistivity coefficients and superconductivity. **a** Pressure p -dependence of the low-temperature T^2 coefficient A_t (circles) obtained from linear fits of the derivative of the resistivity $d\rho/dT$ below 10 K (black lines in Fig. 1c, d). Also shown are the coefficients $A = A_t - A'$ (diamonds), the component of A_t attributed to electron-electron scattering dressed by critical nematic fluctuations. Dashed lines are linear fits to the data. The strengthening superconductivity prevents A_t (and A) from being determined at the highest applied pressures. **b** Pressure dependence of the T -linear coefficient B was obtained by fitting $d\rho/dT$ measured between 20 and 40 K to a straight line. Dashed lines are linear fits to the data. **c** Pressure dependence of the residual resistivity ρ_0 was obtained by extrapolating the low- T $\rho(T)$ curves at 35 T to 0 K. Values were only obtained up to the pressures at which superconducting fluctuations do not influence $\rho(T)$. The dashed lines are extrapolations of straight-line fits to the data points. **d** Pressure dependence of the high- T T^2 coefficient A' as obtained from straight-line fits to $d\rho/dT$ at 35 T and above 20 K. **e** Pressure dependence of the superconducting transition temperature T_c defined as the temperature at which the zero-field resistivity reaches 90% of its value at 35 T. T_c in both samples exhibits an enhancement by a factor of around two. The error bars in panels **a–d** are reflective of the variation of the obtained coefficients to details of the fitting procedure (principally the precise choice of temperature range being fitted to). We estimate there to be an additional 30–50% systematic error due to uncertainty in sample and contact geometry. The error in the obtained values in panel **e** are within the size of the data points.

ρ_0 reflects a change in carrier density (and not a reduction in enhancement from the NQCP). Figure 3a (Fig. 3b) shows the p -dependence of A^* , B^* (A'^*), the coefficients A , B , and A' rescaled by multiplying each quantity by $\rho_0(0)/\rho_0(p)$. As can be seen, the resultant A^* and B^* coefficients are either p -independent (for $x = 0.18$) or fall slightly (for $x = 0.20$) (note, however, the large error bars for the data at highest pressures). The near-constancy and magnitude of $B^*(p)$ is then consistent with the notion that the effective scattering rate remains at the Planckian bound with increasing pressure, in agreement with what had been found at ambient pressures³³. Within a QC scenario, the near-constancy of $A^*(p)$ is also consistent with the fact that the extent of the (low- T) T^2 regime in both samples does not vary with p . This is consistent with pressure tuning parallel to the nematic phase boundary in the p - T plane as indicated in Fig. 3c. By contrast, at ambient pressure A_t exhibits a marked decrease with increasing x beyond the NQCP (see Fig. 3d) while the temperature of the T^2 to T -linear crossover increases as the system is tuned away from the NQCP by chemical substitution^{33,35}.

Discussion

Irrespective of which scenario is the most appropriate, the marked increase in A' (or in A'^*) with pressure, in both samples, is a robust observation. The order of magnitude change in A'^* , in particular, is even greater than that seen in A_t^* upon approach to the NQCP at ambient pressure (Fig. 3d) and comparable to that observed in other quantum critical systems with well-established magnetic

QCPs^{50,54,55}. Moreover, the fact that A' is anti-correlated with A and B implies that the former has a distinct origin. The marked rise in A' is consistent with an enhancement in the quasiparticle-quasiparticle scattering cross-section upon approach to a second, distinct QCP. The absolute magnitude of A' over our experimental pressure range (~ 5 n Ω cm K $^{-2}$), however, is much smaller than the value that A_t reaches (>200 n Ω cm K $^{-2}$)^{33,35} upon approaching the ambient pressure NQCP, as shown in Fig. 3d. This, coupled with the more extended temperature range over which this T^2 term persists, suggests that the second QCP is likely to be situated at a critical pressure far beyond those accessible here. As illustrated in Fig. 2e, the approach to the second QCP also coincides with a marked (factor of 2) growth in T_c for both samples, the growth in A' and T_c being largest for $x = 0.18$. As mentioned in the introduction, a marked increase in T_c with pressure at lower sulfur concentrations has been linked previously to strengthening magnetic interaction³⁰. Indeed, it has been suggested that T_c is maximized at the magnetic QCP⁴³ and it is known that magnetism is stabilized at higher pressures^{43,53}. Although there have been no reports to date confirming the presence of magnetic order with increasing pressure beyond $x_c = 0.17$, resistivity data presented in Matsuura et al.⁴³ show that the magnetic ordering temperature at 5 GPa remains doping independent up to x_c . Thus, it seems reasonable to expect magnetic order to be stabilized under pressure beyond x_c and we associate this second QCP with the pressure-induced anti-ferromagnetic phase, and ascribe the p -dependence of the second T^2 component in $\rho(T)$ to quasiparticle-quasiparticle dressing by critical spin fluctuations in the quantum disordered regime.

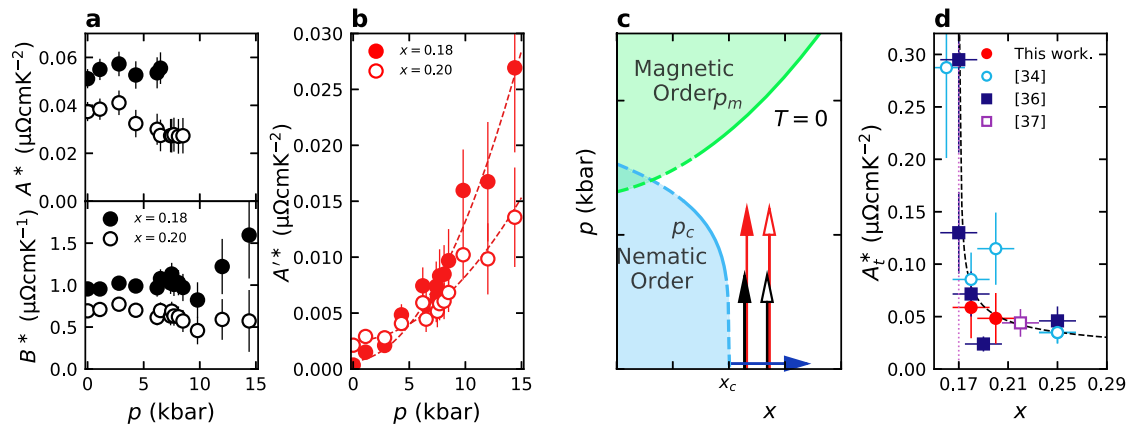


Fig. 3 Decoupled nematic and magnetic criticality in $\text{FeSe}_{1-x}\text{S}_x$. **a** Renormalized A^* coefficient (upper) and similarly renormalized B^* coefficient (lower) as a function of pressure having rescaled A and B respectively by the pressure-induced change in ρ_0 . **b** Similarly renormalized A^* coefficient as a function of pressure. **c** Schematic $T = 0$ phase diagram in the p - x plane showing the nematic and magnetic phase boundaries. Vertical arrows indicate the pressure-induced approach of the two studied samples to the magnetic quantum critical point and the pressure ranges over which A and A^* can be determined. The horizontal arrow represents tuning away from the nematic quantum critical point (NQCP) with increasing x (relevant to panel **d**). Near $x = x_c$, the nematic phase boundary is shown as a dashed line to reflect its putative weak first-order nature. **d** Variation of A_t^* , the total low-temperature T^2 coefficient at ambient pressure rescaled by the relative growth in the carrier density, and x beyond the nematic quantum critical point near $x_c \sim 0.17$ (red dotted line) with data from this work and literature sources^{33,36,37}. The error bars represent the estimated uncertainty in both x and the reported coefficients. We have estimated the error in the values reported in this work to be 50% due to the constraints on sample size in a pressure cell and 30% elsewhere. The uncertainty in x has been assumed to be ± 0.015 and representative of the typical variation in x within an individual batch of samples¹². See Supplementary Note 1 for details of the rescaling procedure. The dashed line is a guide to the eye.

Of course, there are other scattering mechanisms that are capable of generating T^2 resistivity with a variable coefficient, such as non-critical electron–electron scattering near a Mott metal–insulator transition⁵⁶, electron–phonon scattering in disordered systems⁵⁷ or short-range spin fluctuation scattering⁵⁸. However, the order-of-magnitude increase in A^* over a relatively narrow pressure range is difficult to reconcile with any of these mechanisms. One would need to invoke a pressure-induced suppression of disorder by one order of magnitude for electron–phonon scattering to be sufficient⁵⁷, there is no evidence for Mottness and while spin fluctuations are found to be pressure independent in pure FeSe³⁹, they become suppressed with pressure up to 2 GPa (the pressure range of this study) at $x = 0.12$ ⁵⁹. Clearly, further studies will be required to definitively rule out these alternative explanations. However, given the known emergence of a magnetic phase boundary in $\text{FeSe}_{1-x}\text{S}_x$ at higher pressures as well as a precedent for magnetic quantum criticality in other Fe-based⁵⁵ or heavy fermion^{51,54} systems manifesting in a divergent T^2 coefficient of the low- T resistivity, a magnetic QCP seems the most plausible.

These contrasting x - and p -dependencies ($A_t(x)$ and $A^*(p)$) may be reconciled by considering the proposed $T = 0$ phase diagram shown schematically in Fig. 3c. The vertical solid- and open-headed arrows represent, respectively, the pressure tuning of the $x = 0.18$ and 0.20 samples, while the horizontal arrow represents tuning away from the NQCP with increasing x at ambient pressure. The near-constancy of A^* (within the second scenario above) may indicate that $p_c(x)$ —the phase boundary for nematic order in the (p, x) plane—is very steep near $x = x_c$. This seems plausible given the steepness of $T_s(x)$ near x_c —see Fig. 1a in M. Čulo et al.³⁸, for example. Consequently, with increasing p , samples with $x > x_c$ track effectively parallel to the nematic phase boundary, rather than away from it. At the same time, the application of pressure tunes each sample towards $p_m(x)$ —the magnetic phase boundary—resulting in a marked increase in A' . In this way, the contrasting variation in $A(p)$ and $A'(p)$ can be understood. The steepness of the $p_c(x)$ boundary might also indicate a crossover in the nematic phase transition from second-

order to weakly first-order near $x = x_c$. Such a crossover, intimated in Fig. 3c by the dashed nematic phase boundary, would lead to a cutoff in the nematic fluctuations, thereby providing an alternative explanation for the p -independence of A^* and B^* . It is noted that in pure FeSe, $T_s(p)$ terminates at a first-order structural and magnetic phase transition at ~ 2 GPa (a divergence of $1/T_1T$ at low T is lost)⁶⁰. The $T = 0$ endpoint of the magnetic transition, however, appears to remain second-order⁶⁰. Thus one anticipates that the magnetic phase boundary at the higher dopings measured in this study is also second-order and capable of hosting a QCP.

The presence of two anti-correlated but additive T^2 components in the low- T resistivity is unusual but implies the presence of two independent scattering channels of distinct origin. Given the correlation between A' and T_c at finite pressure and the anticorrelation between A' and A , it seems very unlikely that spin fluctuations could be responsible for both. Indeed, while measurements of the spin-lattice relaxation rate in $\text{FeSe}_{1-x}\text{S}_x$ at ambient pressure indicate the emergence of low-lying spin fluctuations below T_s , spin fluctuations are strongly suppressed for $x > x_c$ ³⁹. Moreover, as mentioned above, there is no evidence that such fluctuations go critical at $x = x_c$. It would appear that spin fluctuations, as parameterized by A' ($\sim A_t/10$), play only a minor role in the overall low- T resistivity in $\text{FeSe}_{1-x}\text{S}_x$ at ambient pressure.

The measurements presented here imply that the nematic fluctuations anchored at the NQCP and the magnetic fluctuations anchored at the AFM QCP act as decoupled mechanisms for the enhancement of quasiparticle–quasiparticle scattering over most of the phase diagram of $\text{FeSe}_{1-x}\text{S}_x$. One possible way to account for their distinct nature is to consider the particular Fermi surface topology of $\text{FeSe}_{1-x}\text{S}_x$. Figure 4a shows a schematic projection of the Fermi surface of $\text{FeSe}_{1-x}\text{S}_x$ ($x > x_c$) at $k_z = 0$ assuming only one hole pocket centered at Γ and two-electron pockets at X and Y. Since spin fluctuations in detwinned FeSe are peaked at $\mathbf{Q} = (\pi, 0)$ ¹⁵, we also assume that in the tetragonal phase, critical spin fluctuations would enhance the quasiparticle–quasiparticle scattering cross-section predominantly at four ‘hot-spots’, as shown

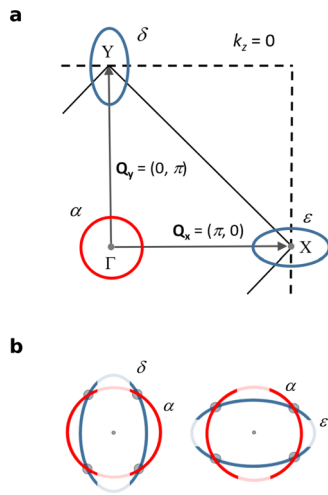


Fig. 4 Decoupling of the nematic and magnetic interactions and the Fermi surface of $\text{FeSe}_{1-x}\text{S}_x$. **a** Schematic Fermi surface of $\text{FeSe}_{1-x}\text{S}_x$ outside of the nematic phase showing the Γ -centered hole pocket (α) and X, Y-centered electron pockets (ϵ and δ) at $k_z = 0$. States on different pockets can be connected via finite- \mathbf{Q} scattering as indicated by the gray arrows. **b** Schematic illustrating the distinct regions of quasiparticle dressing due to critical magnetic fluctuations (grey circles) arising from the translation of the pockets through $\mathbf{Q} = (\pi, 0)$, $(0, \pi)$, and nematic (Pomeranchuk) fluctuations (lighter shaded regions on the electron/hole pockets where the quasiparticle spectral weight is reduced⁶³).

in Fig. 4b. The precise symmetry of the nematic fluctuations in $\text{FeSe}_{1-x}\text{S}_x$ has not yet been confirmed. Raman spectroscopy studies have indicated the presence of a d -wave Pomeranchuk instability^{61,62} while quasiparticle scattering interference experiments⁶³ have revealed a highly anisotropic spectral weight (of different orbital character) on both pockets with p -wave symmetry (lightly shaded sections in Fig. 4b). For the former, critical nematic fluctuations would dress the quasiparticle states everywhere except at the AFM hot-spots (the nodes of the d -wave Pomeranchuk deformation), while for the latter, these cold-spots would reside at the “bellies” of each pocket. Such considerations might then help us to envisage how the influence of the critical nematic or magnetic fluctuations manifests themselves as two distinct components of the T^2 resistivity. Intriguingly, the in-plane magnetoresistance of $\text{FeSe}_{1-x}\text{S}_x$ (at ambient pressure) can also be decomposed into two components³⁵; a QC component that exhibits H/T scaling and is maximal near the NQCP and a second component that remains purely H^2 (up to 35 T) and shows conventional Kohler’s scaling. It is tempting to attribute these two components as arising from these distinct nematic and spin interactions, only one of which goes critical at ambient pressure.

Finally, we turn to consider the evolution of the superconductivity in $\text{FeSe}_{1-x}\text{S}_x$. While there is strong evidence to suggest that low-energy spin-fluctuations play a significant role in the pairing mechanism in $\text{FeSe}_{1-x}\text{S}_x$ ^{23–26}, the increase in $T_c(p)$ appears to be well correlated with $A'(p)$ (panels d, e of Fig. 2), it is striking that $A' \sim A_t/10$ at ambient pressure yet T_c remains high (~ 8 K). This finding may suggest some role for nematicity in the pairing in $\text{FeSe}_{1-x}\text{S}_x$ but clearly, further work is required to confirm this. In pnictide superconductors, where nematicity and magnetism are strongly coupled, superconductivity is most likely driven by low-energy spin fluctuations, though T_c could be enhanced by a reduction in the bare intra-pocket repulsion brought about by the nematic fluctuations⁷. In the case of $\text{FeSe}_{1-x}\text{S}_x$, the decoupling of the nematic and the magnetic

fluctuations means that this cooperative process is no longer viable and as a result, T_c is not enhanced at the NQCP.

Previously, pressure tuning between two distinct QCPs was reported in the heavy-fermion compounds Ge-doped CeCu_2Si_2 ^{64,65} and YbRh_2Si_2 with Ir and Co doping⁶⁶. To the best of our knowledge, however, $\text{FeSe}_{1-x}\text{S}_x$ represents the first example of a correlated metal exhibiting an enhancement in the coefficient of the T^2 resistivity associated with two distinct QCPs. Clearly, the task is now to determine the universality classes associated with each criticality. In order to achieve this, however, it will be necessary to study a sample with a sulfur concentration even closer to the NQCP and to extend the pressure range (e.g., using an anvil cell) until the magnetic QCP itself is crossed. At the same time, determination of the evolution of complementary resistive properties (such as the Hall effect) with pressure may help elucidate further the nature of the two components.

Methods

Samples. Single crystals were grown via a KCl/AlCl₃ chemical vapor transport method. The growth was typically performed with a source temperature of 420 °C, a deposition zone temperature of 230 °C, and with a growth time of 200 h. Their nominal dopings are $x = 0.18$ and 0.20. The actual S content of crystals can often be lower than the nominal value¹². For both of our samples, however, the zero-field $\rho(T)$ curves (at ambient pressure) are found to agree well with previous reports on samples with similar dopings^{33,36,37}. Specifically, there is no kink or minimum in the derivative $d\rho/dT$ that could be attributed to a finite T_s , and the T^2 regime at low- T extends up to around 8–10 K with a coefficient $A_t \sim 40$ –55 n Ω cm K⁻², compared with >200 n Ω cm K⁻² for $x \leq 0.17$ ^{33,36}. In this work, there is heightened geometrical uncertainty associated with measuring small crystals inside a pressure cell. Whilst, the as-measured A_t values are $\sim 25\%$ lower than previous reports at the same nominal doping levels, as is evident from Fig. 3d, the values obtained are in good agreement with the general trend of $A_t(x)$ with data taken from multiple groups (see Supplementary Note 1 for details).

Resistivity measurement under pressure. Resistivity was measured using a standard ac lock-in technique. Electrical contact was made to the samples by first masking the samples and sputtering gold pads. Contact to the pads was made using gold wire and DuPont 4929 silver paint. Typical contact resistances were less than 1 Ω and stable over time. Both crystals were mounted together in a single piston-cylinder pressure cell and oriented such that $\mathbf{H} \parallel \mathbf{I} \parallel ab$. Daphne 7373, which is known to remain hydrostatic at room temperature up to 22 kbar⁶⁷, was used as a pressure transmitting medium. Resistivity measurements were performed using a standard four-point ac lock-in technique in Cell 4 of the High Field Magnet Laboratory (Radboud University, Nijmegen, The Netherlands) where a maximum magnetic field of 35 T could be applied. Temperature sweeps were performed in both field orientations (positive and negative 35 T) such that the longitudinal component could be isolated from any Hall component present due to an offset in the voltage contacts (though it is noted that the Hall contribution was found to be a near-negligible part of the total signal).

Data availability

The data that support the plots within this paper and other findings of this study are available from the University of Bristol data repository, data.bris, at <https://doi.org/10.5523/bris.3spp0cgrmsam924e0xirqckhlf>.

Received: 9 August 2021; Accepted: 10 February 2022;

Published online: 22 April 2022

References

1. Kasahara, S. et al. Evolution from non-Fermi- to Fermi-liquid transport via isovalent doping in $\text{BaFe}_2(\text{As}_{1-x}\text{P}_x)_2$ superconductors. *Phys. Rev. B* **81**, 184519 (2010).
2. Paglione, J. & Greene, R. L. High-temperature superconductivity in iron-based materials. *Nat. Phys.* **6**, 645–658 (2010).
3. McQueen, T. M. et al. Tetragonal-to-orthorhombic structural phase transition at 90 K in the superconductor $\text{Fe}_{1.01}\text{Se}$. *Phys. Rev. Lett.* **103**, 057002 (2009).
4. Sato, Y. et al. Thermodynamic evidence for a nematic phase transition at the onset of the pseudogap in $\text{YBa}_2\text{Cu}_3\text{O}_y$. *Nat. Phys.* **13**, 1074–1078 (2017).
5. Ronning, F. et al. Electronic in-plane symmetry breaking at field-tuned quantum criticality in CeRhIn_5 . *Nature* **548**, 313–317 (2017).

6. Cao, Y. et al. Nematicity and competing orders in superconducting magic-angle graphene. *Science* **379**, 264–271 (2021).
7. Fernandes, R. M., Chubukov, A. V. & Schmalian, J. What drives nematic order in iron-based superconductors? *Nat. Phys.* **10**, 97–104 (2014).
8. Borzi, R. A. et al. Formation of a nematic fluid at high fields in $\text{Sr}_3\text{Ru}_2\text{O}_7$. *Science* **315**, 214–217 (2007).
9. Lester, C. et al. Field-tunable spin-density-wave phases in $\text{Sr}_3\text{Ru}_2\text{O}_7$. *Nat. Mater.* **14**, 373–378 (2015).
10. Tanatar, M. A. et al. Origin of the resistivity anisotropy in the nematic phase of FeSe. *Phys. Rev. Lett.* **117**, 127001 (2016).
11. Sprau, P. O. et al. Discovery of orbital-selective Cooper pairing in FeSe. *Science* **357**, 75–80 (2017).
12. Hosoi, S. et al. Nematic quantum critical point without magnetism in $\text{FeSe}_{1-x}\text{S}_x$ superconductors. *Proc. Natl Acad. Sci. USA* **113**, 8139–8143 (2016).
13. Massat, P. et al. Collapse of critical nematic fluctuations in FeSe under pPressure. *Phys. Rev. Lett.* **121**, 077001 (2018).
14. Baek, S.-H. et al. Orbital-driven nematicity in FeSe. *Nat. Mater.* **14**, 210–214 (2015).
15. Chen, T. et al. Anisotropic spin fluctuations in detwinned FeSe. *Nat. Mater.* **18**, 9 (2019).
16. Wang, Q. et al. Magnetic ground state of FeSe. *Nat. Commun.* **7**, 12182 (2016).
17. Oganeyan, V., Kivelson, S. A. & Fradkin, E. Quantum theory of a nematic Fermi fluid. *Phys. Rev. B* **64**, 195109 (2001).
18. Maslov, D. L., Yudson, V. I. & Chubukov, A. Resistivity of a non-Galilean-invariant Fermi liquid near Pomeranchuk quantum criticality. *Phys. Rev. Lett.* **106**, 106403 (2011).
19. Hartnoll, S., Mahajan, R., Punk, M. & Sachdev, S. Transport near the Ising-nematic quantum critical point of metals in two dimensions. *Phys. Rev. B* **89**, 155130 (2014).
20. Lederer, S., Schattner, Y., Berg, E. & Kivelson, S. A. Superconductivity and non-Fermi liquid behavior near a nematic quantum critical point. *Proc. Natl Acad. Sci. USA* **114**, 4905–4910 (2017).
21. Wang, X. & Berg, E. Scattering mechanisms and electrical transport near an Ising nematic quantum critical point. *Phys. Rev. B* **99**, 235136 (2019).
22. de Carvalho, V. S. & Fernandes, R. M. Resistivity near a nematic quantum critical point: impact of acoustic phonons. *Phys. Rev. B* **100**, 115103 (2019).
23. Böhmer, A. E. & Kreisel, A. Nematicity, magnetism and superconductivity in FeSe. *J. Phys. Condens. Matter* **30**, 023001 (2018).
24. Coldea, A. I. & Watson, M. D. The key ingredients of the electronic structure of FeSe. *Annu. Rev. Condens. Matter Phys.* **9**, 125–146 (2018).
25. Kriesel, A., Hirschfeld, P. J. & Andersen, B. M. On the remarkable superconductivity of FeSe and its close cousins. *Symmetry* **12**, 1402 (2020).
26. Shibauchi, T., Hanaguri, T. & Matsuda, Y. Exotic superconducting states in FeSe-based materials. *J. Phys. Soc. Jpn.* **89**, 102002 (2020).
27. Sun, J. P. et al. Dome-shaped magnetic order competing with high-temperature superconductivity at high pressures in FeSe. *Nat. Commun.* **7**, 12146 (2016).
28. Medvedev, S. et al. Electronic and magnetic phase diagram of $\beta\text{-Fe}_{1.01}\text{Se}$ with superconductivity at 36.7 K under pressure. *Nat. Mater.* **8**, 630–633 (2009).
29. Margadonna, S. et al. Pressure evolution of the low-temperature crystal structure and bonding of the superconductor FeSe ($T_c = 37$ K). *Phys. Rev. B* **80**, 064506 (2009).
30. Imai, T., Ahilan, K., Ning, F. L., McQueen, T. M. & Cava, R. J. Why does undoped FeSe become a high- T_c superconductor under pressure? *Phys. Rev. Lett.* **102**, 177005 (2009).
31. Bendele, M. et al. Pressure induced static magnetic order in superconducting FeSe_{1-x} . *Phys. Rev. Lett.* **104**, 087003 (2010).
32. Watson, M. D. et al. Suppression of orbital ordering by chemical pressure in $\text{FeSe}_{1-x}\text{S}_x$. *Phys. Rev. B* **92**, 121108 (2015).
33. Licciardello, S. et al. Electrical resistivity across a nematic quantum critical point. *Nature* **567**, 213–217 (2019).
34. Urata, T. et al. Non-Fermi liquid behavior of electrical resistivity close to the nematic critical point in $\text{Fe}_{1-x}\text{Co}_x\text{Se}$ and $\text{FeSe}_{1-y}\text{S}_y$. Preprint at [arXiv:1608.01044](https://arxiv.org/abs/1608.01044) [cond-mat.supr-con] (2016).
35. Licciardello, S. et al. Coexistence of orbital and quantum critical magnetoresistance in $\text{FeSe}_{1-x}\text{S}_x$. *Phys. Rev. Res.* **1**, 023011 (2019).
36. Bristow, M. et al. Anomalous high-magnetic field electronic state of the nematic superconductors $\text{FeSe}_{1-x}\text{S}_x$. *Phys. Rev. Res.* **2**, 013309 (2020).
37. Huang, W. K. et al. Non-Fermi liquid transport in the vicinity of the nematic quantum critical point of superconducting $\text{FeSe}_{1-x}\text{S}_x$. *Phys. Rev. Res.* **2**, 033367 (2020).
38. Čulo, M. et al. Putative Hall response of the strange metal sector in $\text{FeSe}_{1-x}\text{S}_x$. *Phys. Rev. Res.* **3**, 023069 (2021).
39. Wiecki, P. et al. Persistent correlation between superconductivity and antiferromagnetic fluctuations near a nematic quantum critical point in $\text{FeSe}_{1-x}\text{S}_x$. *Phys. Rev. B* **98**, 020507 (2018).
40. Coldea, A. I. et al. Evolution of the low-temperature Fermi surface of superconducting $\text{FeSe}_{1-x}\text{S}_x$ across a nematic phase transition. *npj Quant. Mater.* **4**, 2 (2019).
41. Paul, I. & Garst, M. Lattice effects on nematic quantum criticality in metals. *Phys. Rev. Lett.* **118**, 227601 (2017).
42. Wiecki, P. et al. NMR evidence for static local nematicity and its cooperative interplay with low-energy magnetic fluctuations in FeSe under pressure. *Phys. Rev. B* **96**, 180502 (2017).
43. Matsuura, K. et al. Maximizing T_c by tuning nematicity and magnetism in $\text{FeSe}_{1-x}\text{S}_x$ superconductors. *Nat. Commun.* **8**, 1143 (2017).
44. Kuwayama, T. et al. Magnetic fluctuations under pressure on S-doped FeSe studied via ^{77}Se NMR. *AIP Adv.* **8**, 101308 (2018).
45. Reiss, P. et al. Quenched nematic criticality and two superconducting domes in an iron-based superconductor. *Nat. Phys.* **16**, 89–94 (2020).
46. Holenstein, S. et al. Extended magnetic dome induced by low pressures in superconducting $\text{FeSe}_{1-x}\text{S}_x$. *Phys. Rev. Lett.* **123**, 147001 (2019).
47. Yip, K. Y. et al. Weakening of the diamagnetic shielding in $\text{FeSe}_{1-x}\text{S}_x$ at high pressures. *Phys. Rev. B* **96**, 020502 (2017).
48. Ayres, J. *Correlated Electron Systems Under Extreme Conditions: High Fields, High Pressures, Low Temperatures*. PhD thesis, The University of Bristol (2020).
49. Xiang, L. et al. Dome of magnetic order inside the nematic phase of sulfur-substituted FeSe under pressure. *Phys. Rev. B* **96**, 024511 (2017).
50. Grigera, S. A. et al. Magnetic field-tuned quantum criticality in the metallic ruthenate $\text{Sr}_3\text{Ru}_2\text{O}_7$. *Science* **294**, 329–332 (2001).
51. Custers, J. et al. The break-up of heavy electrons at a quantum critical point. *Nature* **424**, 4 (2003).
52. Shibauchi, T., Carrington, A. & Matsuda, Y. A quantum critical point lying beneath the superconducting dome in iron pnictides. *Annu. Rev. Condens. Matter Phys.* **5**, 113–135 (2014).
53. Terashima, T. et al. Pressure-induced antiferromagnetic transition and phase diagram in FeSe. *J. Phys. Soc. Jpn.* **84**, 063701 (2015).
54. Gegenwart, P. et al. Magnetic-field induced quantum critical point in YbRh_2Si_2 . *Phys. Rev. Lett.* **89**, 056402 (2002).
55. Analytis, J. G. et al. Transport near a quantum critical point in $\text{BaFe}_2(\text{As}_{1-x}\text{P}_x)_2$. *Nat. Phys.* **10**, 194–197 (2014).
56. Tokura, Y. et al. Filling dependence of electronic properties on the verge of metal–Mott-insulator transition in $\text{Sr}_{1-x}\text{La}_x\text{TiO}_3$. *Phys. Rev. Lett.* **70**, 2126–2129 (1993).
57. Gurvitch, M., Ghosh, A. K., Lutz, H. & Strongin, M. Low-temperature resistivity of ordered and disordered A15 compounds. *Phys. Rev. B* **22**, 128–136 (1980).
58. Ihle, D. & Plakida, N. M. Spin-fluctuation resistivity in high-temperature superconductors. *Phys. C: Superconductivity*. **185–189**, 1637–1638 (1991).
59. Kuwayama, T. et al. ^{77}Se -NMR study under pressure on 12%-S doped FeSe. *J. Phys. Soc. Jpn.* **88**, 033703 (2019).
60. Wang, P. S. et al. Pressure induced stripe-order antiferromagnetism and first-order phase transition in FeSe. *Phys. Rev. Lett.* **117**, 237001 (2016).
61. Zhang, W.-L. et al. Stripe quadrupole order in the nematic phase of $\text{FeSe}_{1-x}\text{S}_x$. *Proc. Natl Acad. Sci. USA* **118**, e2020585118 (2021).
62. Chibani, S. et al. Lattice-shifted nematic quantum critical point in $\text{FeSe}_{1-x}\text{S}_x$. *npj Quant. Mat.* **6**, 37 (2021).
63. Kostin, A. et al. Imaging orbital-selective quasiparticles in the Hund’s metal state of FeSe. *Nat. Mater.* **17**, 869–874 (2018).
64. Yuan, H. Q. et al. Observation of two distinct superconducting phases in CeCu_2Si_2 . *Science* **302**, 2104–2107 (2003).
65. Yuan, H. Q. et al. Non-Fermi liquid states in the pressurized $\text{CeCu}_2(\text{Si}_{1-x}\text{Ge}_x)_2$ system: two critical points. *Phys. Rev. Lett.* **96**, 047008 (2006).
66. Friedemann, S. et al. Detaching the antiferromagnetic quantum critical point from the Fermi-surface reconstruction in YbRh_2Si_2 . *Nat. Phys.* **5**, 465–469 (2009).
67. Yokogawa, K., Murata, K., Yoshino, H. & Aoyama, S. Solidification of high-pressure medium Daphne 7373. *Jpn. J. Appl. Phys.* **46**, 3636–3639 (2007).

Acknowledgements

The authors acknowledge enlightening discussions with M. Berben, C. Duffy, B. Gou-téreaux, R. Hinlopen, Y.-T. Hsu, and C. Pépin. J.A. acknowledges the support of the EPSRC-funded CMP-CDT (Ref. EP/L015544/1) and an EPSRC Doctoral Prize Fellowship (Ref. EP/T517872/1). A.C. and S.F. acknowledge the support of the EPSRC (Ref. EP/R011141/1). We also acknowledge the support of the High Field Magnet Laboratory (HFML) at Radboud University (RU), member of the European Magnetic Field Laboratory (EMFL), and the former Foundation for Fundamental Research on Matter (FOM), which is financially supported by the Netherlands Organization for Scientific Research (NWO) (Grant No. 16METL01), “Strange Metals.” Part of this work was also supported by the European Research Council (ERC) under the European Union’s Horizon 2020 research and innovation program (Grant Agreements no. 835279-Catch-22 and 715262-HPSuper). This work was also supported by Grants-in-Aid for Scientific

Research (KAKENHI) and in Innovative Areas “Topological Material Science” (No. JP15H05852) and “Quantum Liquid Crystals” (No. JP19H05824) from the Japan Society for the Promotion of Science (JSPS) and by the Japan Science and Technology Agency (JST) CREST program (Grant No. JPMJCR19T5).

Author contributions

J.A. and N.E.H. conceived the project. N.E.H., S.F., and A.C. supervised the project. J.A. prepared the pressure cells with the guidance of S.F. J.A., M.C., J.B., and B.B. performed the high-field measurements. S.K., Y.M., and T.S. grew and characterized the single crystal samples. J.A. and N.E.H. wrote the manuscript with input from all of the co-authors.

Competing interests

The authors declare no competing interests.

Additional information

Supplementary information The online version contains supplementary material available at <https://doi.org/10.1038/s42005-022-00873-8>.

Correspondence and requests for materials should be addressed to Jake Ayres or Nigel E. Hussey.

Peer review information *Communications Physics* thanks the anonymous reviewers for their contribution to the peer review of this work. Peer reviewer reports are available.

Reprints and permission information is available at <http://www.nature.com/reprints>

Publisher's note Springer Nature remains neutral with regard to jurisdictional claims in published maps and institutional affiliations.



Open Access This article is licensed under a Creative Commons Attribution 4.0 International License, which permits use, sharing, adaptation, distribution and reproduction in any medium or format, as long as you give appropriate credit to the original author(s) and the source, provide a link to the Creative Commons license, and indicate if changes were made. The images or other third party material in this article are included in the article's Creative Commons license, unless indicated otherwise in a credit line to the material. If material is not included in the article's Creative Commons license and your intended use is not permitted by statutory regulation or exceeds the permitted use, you will need to obtain permission directly from the copyright holder. To view a copy of this license, visit <http://creativecommons.org/licenses/by/4.0/>.

© The Author(s) 2022